



Synthesis of metal-metal oxide ($Me-Me_nO_m$) nanocomposites by partial reduction and cold sintering

Aliya Sharipova^{a,b,*}, Viacheslav Slesarenko^c, Elazar Gutmanas^{a,1}

^a Department of Materials Science and Engineering, Technion, Haifa 3200003, Israel

^b Institute of Strength Physics and Materials Science, SB RAS, Tomsk 634021, Russia

^c Lavrentyev Institute of Hydrodynamics, SB RAS, Novosibirsk 630090, Russia

ARTICLE INFO

Article history:

Received 29 February 2020

Received in revised form 5 June 2020

Accepted 20 June 2020

Available online 23 June 2020

In memory of our mentor, colleague, friend
– Prof. Emer. Elazar Y. Gutmanas

Keywords:

Metal matrix nanocomposites

Partial reduction

Cold sintering

Core-shell nanoparticles

Fe- Fe_nO_m

ABSTRACT

Metal matrix nanocomposites (MMNCs) require the development of new manufacturing techniques that enable enhanced control over their microstructure and mechanical performance. The approach for MMNC fabrication proposed in this work combines the partial reduction of the oxide nanopowder with the subsequent cold sintering. We show that it is possible to avoid unwanted structural changes such as grain coarsening and inclusion agglomeration. We reveal that a core-shell structure of partially reduced Fe_2O_3 particles facilitates reliable sintering and enables the fabrication of near-dense MMNCs reinforced by iron oxide nanoparticles. The fabricated composites exhibit a homogeneous distribution of reinforcing oxide inclusions and demonstrate high mechanical strength.

© 2020 Elsevier B.V. All rights reserved.

1. Introduction

Metal matrix nanocomposites (MMNCs) have started to gain the attention of various industries due to their superior performance, particularly high strength and better fatigue resistance, as compared to conventional composites [1]. Since the extreme properties of MMNCs originate from their nanostructure, the classical high-temperature powder processing techniques, usually accompanied by barely controllable changes in nanostructure (grain coarsening, clustering of reinforcing inclusions), do not unlock the full potential of MMNCs. Therefore lower-temperature equal channel angular pressing (ECAP) [2] and spark-plasma sintering (SPS) with a high sintering rate [3] were adopted for MMNC fabrication. High-pressure consolidation/cold sintering (CS) might be considered as a promising process for MMNC fabrication thanks to achievements in the synthesis of iron-based composites [4] and ceramic-polymer nanocomposites [5].

While typical MMNC reinforcing inclusions are carbon nanotubes, nitride or oxide particles [6], here we employ fine particles of matrix-metal oxide as a reinforcing agent. To the best of our

knowledge, MMNCs of such type have not been reported before. Here, we propose a method for metal-metal oxide ($Me - Me_nO_m$) nanocomposite fabrication by partial reduction of oxide nanopowder followed by cold sintering (Fig. 1). At the first step, partial reduction of oxide nanopowder results in the formation of particles with core (oxide) – shell (metal) structure. During the second step, cold sintering leads to the particle consolidation into bulk $Me - Me_nO_m$ nanocomposite.

The proposed technique helps to circumvent unwanted alternation of MMNC structure and enables a homogeneous distribution of the core phase (oxide) at a nanoscale level (Fig. 1). The metallic outer phase prevents agglomeration of the core phase and its clustering at the grain boundaries. In addition, the nature of the redox reaction provides robust bonding at the metal-oxide interface [7]. All these advantages shall result in $Me - Me_nO_m$ MMNCs with improved properties.

2. Materials and methods

We demonstrate the benefits of proposed MMNC fabrication technique on an example of $Fe - Fe_nO_m$ nanocomposite. Fe_2O_3 nanopowder (<50 nm, Sigma-Aldrich, $\gamma - Fe_2O_3$) was consolidated at 100 MPa into 50%-dense compacts. Partial reduction of the compacts was performed in ultra-high purity hydrogen (H_2 99.999%) at

* Corresponding author at: Department of Materials Science and Engineering, Technion, Haifa 3200003, Israel.

E-mail address: sharipova@campus.technion.ac.il (A. Sharipova).

¹ Deceased 26 October 2019.

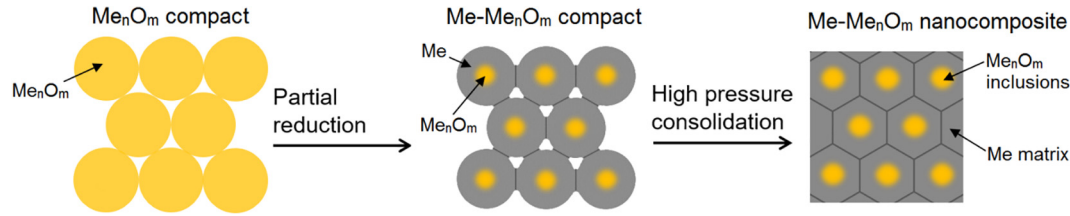


Fig. 1. Fabrication of $Me - Me_nO_m$ MMNC by CS of partially reduced oxide nanopowder.

a flow of $0.13 \text{ cm}^3/\text{s}$ ($325 \text{ }^\circ\text{C}$, 165 min). Under these conditions, the compact loses 28.5 wt% of its mass.

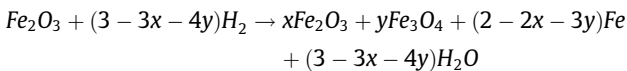
Fe_2O_3 reduction at temperatures below $570 \text{ }^\circ\text{C}$ is usually a two-step process of $Fe_2O_3 \rightarrow Fe_3O_4$ the intermediate reaction followed by $Fe_3O_4 \rightarrow Fe$ reduction [8]. However, the kinetics of Fe_2O_3 reduction is highly dependent on process parameters, and even a direct reduction $Fe_2O_3 \rightarrow Fe$ in pure hydrogen atmosphere at temperatures below $380 \text{ }^\circ\text{C}$ can occur [9]. To remove the ambiguity we adopt the notion $Fe - Fe_nO_m$ to refer the obtained compacts without mentioning exact composition of the oxide core consisting of mix of Fe_2O_3 and Fe_3O_4 oxides (section 3.1). To prepare near to dense specimens, partially reduced compacts were consolidated at 3.0 GPa in preheated to $300 \text{ }^\circ\text{C}$ tungsten carbide die.

The microstructure of the samples was studied with the aid of X-ray diffractometry (XRD, Philips PW-1820 with $\text{Cu K}\alpha$ radiation) and of high-resolution scanning electron microscopy (HR SEM, Zeiss Ultra+) with backscattered electron (BSE) and energy-dispersive (EDS) detectors for phase and microstructure characterization. Bulk samples were etched by H_2NO_3 1.6% solution for structure characterization. The density of bulk samples was determined by the Archimedes method. Compression tests were performed using Instron-1195 testing machine on $5 \times 4 \text{ mm}$ (diameter \times thickness) specimens at a strain rate of 10^{-5} s^{-1} .

3. Results and discussions

3.1. Evaluation of $Fe - Fe_nO_m$ composition after partial reduction

The balanced equation of Fe_2O_3 reduction at the temperatures below $570 \text{ }^\circ\text{C}$ can be written as



where x and y are coefficients of Fe_2O_3 and Fe_3O_4 in the reaction products, respectively. Monte Carlo simulations for a range of the admissible (x, y) values showed that the volume fraction of the residual oxide in the product is bounded by two reactions (Fig. 2a). Lower estimate corresponds to the direct $Fe_2O_3 \rightarrow Fe$ reduction, while the upper bound corresponds to the sequence $Fe_2O_3 \rightarrow Fe_3O_4 \rightarrow Fe$ with a complete transformation of Fe_2O_3 to Fe_3O_4 at the initial step. The explicit expressions connecting mass reduction m and volume fraction of residual oxides V derived for lower and upper bounds take the form

$$V = \frac{1}{1 + \frac{\rho(Fe_2O_3)}{\rho(Fe)} \cdot \frac{mw(Fe_2O_3)}{1-w(Fe_2O_3)-m}} \quad (1)$$

and

$$V = \begin{cases} 1, & \text{if } m \leq m_c \\ \frac{1}{1 + \frac{\rho(Fe_3O_4)}{\rho(Fe)} \cdot \frac{m-m_c w(Fe_3O_4)}{1-w(Fe_3O_4)-\frac{m-m_c}{1-m_c}}}, & \text{if } m > m_c \end{cases} \quad (2)$$

where ρ is the density (g/cm^3), w – the mass fraction of Fe in the corresponding composition, and m_c – mass reduction after the complete transition from Fe_2O_3 to Fe_3O_4 calculated as

$$m_c = \frac{M(O)}{6M(Fe) + 9M(O)} \approx 0.0334, \quad (3)$$

where $M(Fe)$ and $M(O)$ are the molar masses of iron and oxygen (g/mole), respectively.

According to Fig. 2a, the mass loss measurements provide a relatively accurate estimation of the compact composition regardless of the specific reduction path. For the obtained material with a mass loss of 28.5 wt% (denoted as $Fe - Fe_nO_m$), the volume fraction of oxides is between 10.5% and 11.5%.

3.2. Synthesis and characterization of $Fe - Fe_nO_m$ nanocomposites

XRD (Fig. 2b) and EDS (not provided) analyses of the initial nanopowder revealed $\gamma - Fe_2O_3$ stoichiometric composition. XRD analysis of the cold-sintered $Fe - Fe_nO_m$ (Fig. 2b) detected iron and iron oxide peaks that demonstrate broadening due to the nanoscale structure. It is hard to resolve $\gamma - Fe_2O_3$ and Fe_3O_4 by XRD analysis due to very similar patterns [10]. According to simulations, the specific composition of the partially reduced to 28.5 wt % oxide was within a narrow envelope of $Fe - Fe_2O_3 - Fe_3O_4$ compositions. Further investigation by the high-resolution transmission electron microscopy would enable inferring definitive conclusions on the composition of the oxide phase.

High-resolution SEM images of the initial Fe_2O_3 powder and compact after partial reduction are presented in Fig. 3a, b. Careful inspection of the samples did not reveal signs of nanostructure coarsening after the heat treatment. Herewith, we observed partial sintering of nanoparticles, pointed by arrows in Fig. 3b. These findings correlate with studies on reduction of Fe_2O_3 nanopowders, where sintering of 30 nm particles starts at $200 \text{ }^\circ\text{C}$ [11], while sintering of $1-2 \text{ }\mu\text{m}$ particles requires temperatures above $415 \text{ }^\circ\text{C}$ [12]. Besides the nanostructure preservation, low-temperature treatment enabled control over mass loss through the reduction time, which was crucial at a high reduction extent of 28.5%.

High-resolution SEM image of $Fe - Fe_nO_m$ nanocomposite prepared by CS of the partially reduced compact is shown in Fig. 3c. The bright right side shows an as-obtained sample surface; the dark left side reveals the etched site. We observed a system of interconnected nanopores on the sample surface but not in the interior. The average density of the samples was $7.60 \text{ g}/\text{cm}^3$ that is near to 96% of $Fe - Fe_nO_m$ theoretical density. Therefore, the porosity of near 4% likely originates from nanopores on the surface.

Along with exposure of the dense interior, surface etching unveiled nanocomposite structure of the sample (Fig. 3d, e). Close examination of the nanocomposite (Fig. 3d) revealed dark nanoscale inclusions corresponding to oxide phase (Fe_nO_m) in the bright matrix corresponding to Fe phase. This observation confirms that the partial reduction of Fe_2O_3 nanoparticles at the employed conditions lead to the formation of nanoparticles with Fe shell and Fe_nO_m

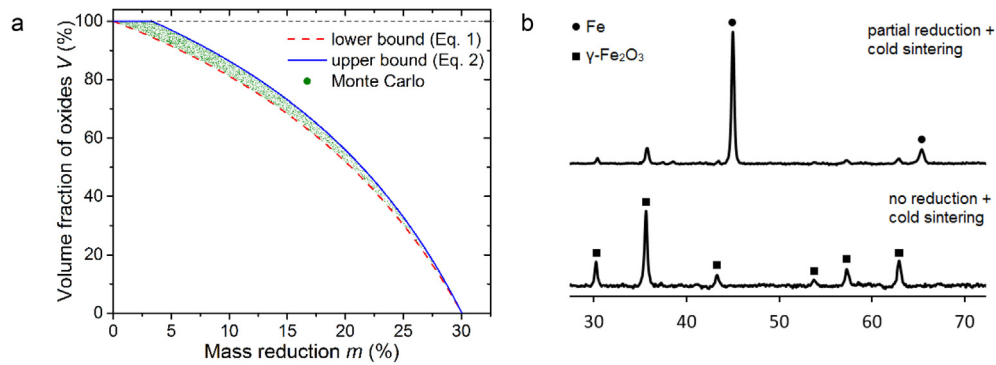


Fig. 2. a) Dependencies of oxide volume fraction on measured mass reduction for all admissible routes of Fe_2O_3 reduction; b) XRD patterns of the initial and the partially reduced to 28.5 wt% Fe_2O_3 nanopowder, both cold-sintered at 3 GPa.

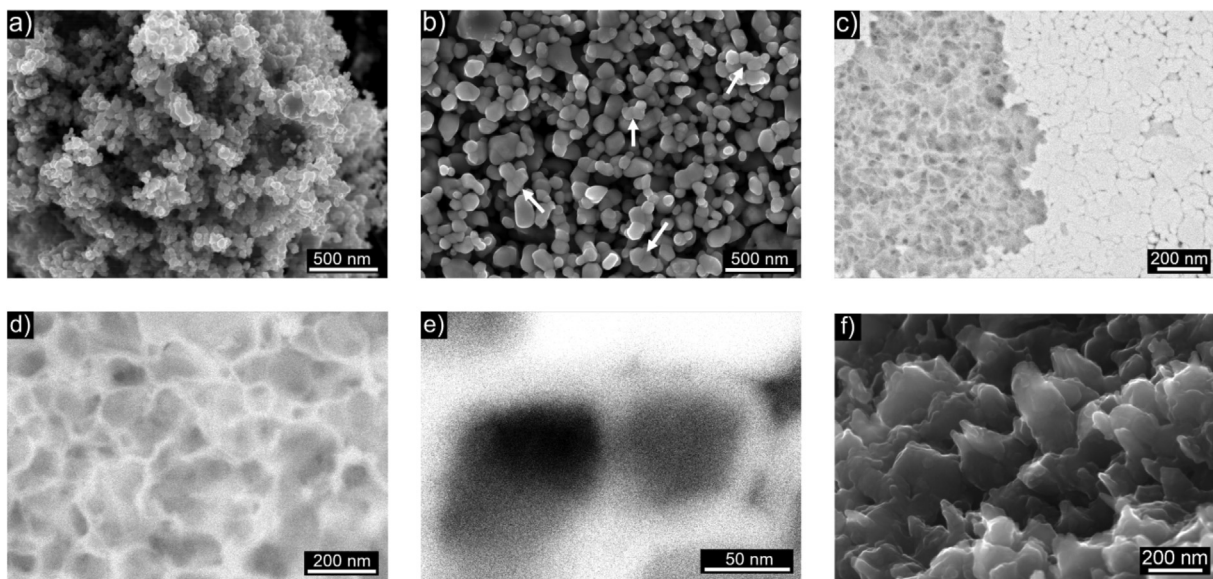


Fig. 3. HR SEM images of (a) Fe_2O_3 initial powder, (b) $Fe-Fe_nO_m$ compact after partial reduction, (c) $Fe-Fe_nO_m$ nanocomposite after CS (BSE), (d, e) $Fe-Fe_nO_m$ nanocomposite, etched site (BSE), (f) $Fe-Fe_nO_m$ nanocomposite, fractured site.

core. Due to the core-shell structure of the grains, oxide inclusions were homogeneously distributed within the metal matrix at the nanoscale level with no agglomeration near grain boundaries of metal phase (Fig. 3c-e), typical in MMNCs fabricated by conventional methods [1,13]. The average size of Fe shell of about 26 nm, estimated from XRD peak broadening (Fig. 2b), correlates with the size of Fe phase observed in HR SEM image (Fig. 3d).

Thanks to nanoscale structure, the measured compressive yield strength of 1035 MPa was 4-fold higher than the previously reported strength of microstructured $Fe-10Fe_2O_3$ obtained by SPS [14]. The appearance of elongated grains and narrowed edges prior to failure in Fig. 3f, similar to previously reported in plastically deformed nanocrystalline Fe [15], can be attributed to the process of ductile failure. Since iron oxides show brittle behavior even at high temperatures (significantly exceeding the testing temperature of 25 °C) [16], the fabricated MMNCs are capable to demonstrate ductile behavior thanks to the presence of Fe phase after the partial reduction.

4. Summary

We proposed a new technique for the fabrication of $Me-Me_nO_m$ nanocomposites by combining partial reduction with cold sintering. On the example of $Fe-Fe_nO_m$ nanocomposite, it was

shown that this technique helps to avoid unwanted structural changes, such as grain coarsening or accumulation of the reinforcing phase at the grain boundaries. Resulted composites had a near-dense structure and demonstrated high mechanical strength. We believe that this technique can be adapted for other reinforcing agents (nitrides, carbides, borides, etc.), and encourage researchers to employ it for MMNCs fabrication.

CRediT authorship contribution statement

Aliya Sharipova: Investigation, Writing - original draft, Visualization. **Viacheslav Slesarenko:** Formal analysis, Writing - original draft. **Elazar Gutmanas:** Conceptualization, Supervision.

Declaration of Competing Interest

The authors declare that they have no known competing financial interests or personal relationships that could have appeared to influence the work reported in this paper.

Acknowledgements

The work was supported by the Ministry of Science & Technology, Israel (grant 3-16574), and by Russian Foundation for Basic

Research (grant 19-53-06006). AS thanks Prof. Eugen Rabkin for support and careful reading of the manuscript. VS thanks the support of state task FWGG-2019-0003.

References

- [1] R. Casati, M. Vedani, Metal matrix composites reinforced by nano-particles – A review, *Metals (Basel)* 4 (2014) 65–83, <https://doi.org/10.3390/met4010065>.
- [2] R. Casati, M. Vedani, D. Dellasega, P. Bassani, A. Tuissi, Consolidated Al/Al₂O₃ nanocomposites by equal channel angular pressing and hot extrusion, *Mater. Manuf. Process.* 30 (2015) 1218–1222, <https://doi.org/10.1080/10426914.2014.912305>.
- [3] N. Saheb, Z. Iqbal, A. Khalil, A.S. Hakeem, N. Al Aqeeli, T. Laoui, A. Al-Qutub, R. Kirchner, Spark plasma sintering of metals and metal matrix nanocomposites: A review, *J. Nanomater.* (2012), <https://doi.org/10.1155/2012/983470>.
- [4] A.F. Sharipova, S.G. Psakhye, I. Gotman, M.I. Lerner, A.S. Lozhkomoev, E.Y. Gutmanas, Cold Sintering of Fe–Ag and Fe–Cu nanocomposites by consolidation in the high-pressure gradient, *Russ. J. Non-Ferrous Met.* 60 (2019) 162–168, <https://doi.org/10.3103/S1067821219020123>.
- [5] J. Guo, A.L. Baker, H. Guo, M. Lanagan, C.A. Randall, Cold sintering process: a new era for ceramic packaging and microwave device development, *J. Am. Ceram. Soc.* 100 (2017) 669–677, <https://doi.org/10.1111/jace.14603>.
- [6] A.D. Moghadam, B.F. Schultz, J.B. Ferguson, E. Omrani, P.K. Rohatgi, N. Gupta, Functional metal matrix composites: Self-lubricating, self-healing, and nanocomposites-an outlook, *JOM* 66 (2014) 872–881, <https://doi.org/10.1007/s11837-014-0948-5>.
- [7] S. Meng, J. Wu, L. Zhao, H. Zheng, S. Jia, S. Hu, W. Meng, S. Pu, D. Zhao, J. Wang, Atomistic insight into the redox reactions in Fe/oxide core-shell nanoparticles, *Chem. Mater.* 30 (2018) 7306–7312, <https://doi.org/10.1021/acs.chemmater.8b03679>.
- [8] D. Spreitzer, J. Schenk, Reduction of iron oxides with hydrogen—a review, *Steel Res. Int.* 90 (2019), <https://doi.org/10.1002/srin.201900108>.
- [9] W.K. Jozwiak, E. Kaczmarek, T.P. Maniecki, W. Ignaczak, W. Maniukiewicz, Reduction behavior of iron oxides in hydrogen and carbon monoxide atmospheres, *Appl. Catal. A Gen.* 326 (2007) 17–27, <https://doi.org/10.1016/j.apcata.2007.03.021>.
- [10] S. Liu, K. Yao, L.H. Fu, M.G. Ma, Selective synthesis of Fe₃O₄, γ -Fe₂O₃, and α -Fe₂O₃ using cellulose-based composites as precursors, *RSC Adv.* 6 (2016) 2135–2140, <https://doi.org/10.1039/c5ra22985e>.
- [11] A.D. Franklin, R.B. Campbell, Low temperature reduction of iron oxides, *J. Phys. Chem.* 59 (1955) 65–67, <https://doi.org/10.1021/j150523a018>.
- [12] A. Pineau, N. Kanari, I. Gaballah, Kinetics of reduction of iron oxides by H₂. Part I: Low temperature reduction of hematite, *Thermochim. Acta.* 447 (2006) 89–100, <https://doi.org/10.1016/j.tca.2005.10.004>.
- [13] A. Saboori, S.K. Moheimani, M. Dadkhah, M. Pavese, C. Badini, P. Fino, An overview of key challenges in the fabrication of metal matrix nanocomposites reinforced by graphene nanoplatelets, *Metals (Basel)* 8 (2018), <https://doi.org/10.3390/met8030172>.
- [14] J. Cheng, T. Huang, Y.F. Zheng, Microstructure, mechanical property, biodegradation behavior, and biocompatibility of biodegradable Fe-Fe₂O₃ composites, *J. Biomed. Mater. Res. – Part A* 102 (2014) 2277–2287, <https://doi.org/10.1002/jbm.a.34882>.
- [15] G. Vetterick, A.C. Leff, M. Marshall, J.K. Baldwin, A. Misra, K. Hattar, M.L. Taheri, Direct observation of a coincident dislocation- and grain boundary-mediated deformation in nanocrystalline iron, *Mater. Sci. Eng., A* 709 (2018) 339–348, <https://doi.org/10.1016/j.msea.2017.09.020>.
- [16] Y. Hidaka, T. Anraku, N. Otsuka, Deformation of iron oxides upon tensile tests at 600–1250°C, *Oxid. Met.* 59 (2003) 97–113, <https://doi.org/10.1023/A:1023070016230>.